Applied Clay Science 97–98 (2014) 62–71

Contents lists available at ScienceDirect

Applied Clay Science

journal homepage: www.elsevier.com/locate/clay

Research paper

# Structure and dynamic properties of water saturated CTMA-montmorillonite: molecular dynamics simulations

Qing Zhou [a,b], Wei Shen [a,b], Jianxi Zhu [a,*], Runliang Zhu [a], Hongping He [a], Jinhong Zhou [a,b], Peng Yuan [a]

[a] Key Laboratory of Mineralogy and Metallogeny, Guangzhou Institute of Geochemistry, Chinese Academy of Sciences, Guangzhou 510640, China
[b] University of Chinese Academy of Sciences, Beijing 100049, China

ARTICLE INFO

*Article history:*
Received 12 December 2013
Received in revised form 26 May 2014
Accepted 31 May 2014
Available online 20 June 2014

*Keywords:*
Organo-montmorillonite
Molecular dynamic
Water saturated condition
Interlayer structures
Mobility
Confining effect

ABSTRACT

The interlayer structure of wet organoclays has attracted great interest due to its close relation with adsorption process but still remains ambiguous at the atomic level. In this study, the structure and dynamics of cetyltrimethylammonium ($CTMA^+$) intercalated montmorillonite (Mt) in the water saturated condition were investigated by molecular dynamics (MD) simulations. Two Mt models with different cation exchange capacity (CEC) were selected and various amounts of $CTMA^+$ were added to achieve different loading levels based on experiments. The simulation results show that as the surfactant loading level increases, the arrangement of $CTMA^+$ transforms from bilayer to inclined paraffin-type with a large amount of water in the interlayer space, indicating a different configuration from dry systems. The conformations of $CTMA^+$ are influenced by water molecules and surfactant loading level. Compared to the dry models, the percentage of *gauche* conformations of $CTMA^+$ decreases in the water saturated condition. In the cases of incomplete cation exchange, the confinement from silicate surface may lead to more ordered structure of alkyl chains. In the cases of excessive surfactant loading, the percentage of *gauche* conformation decreases due to the steric hindrance. Moreover, the ammonium head groups of $CTMA^+$ are found to locate close to the center of six-member ring of silicate surface and coordinated with 4–6 water molecules. Their mobility is low due to the electrostatic interactions while the alkyl chains show higher mobility. Mt with a higher CEC has a stronger confining effect on both alkylammonium and water, which then reduces the mobility of alkyl chains and water molecules within the interlayer space.



## 1. Introduction

Organoclays (OC) synthesized by intercalating alkylammonium ions into clay minerals interlayer spaces have shown excellent adsorption capability toward hydrophobic organic compounds, and attracted great interest in various pollution control fields such as soil remediation and wastewater treatment (Bergaya et al., 2006; Meier et al., 2001; Sheng et al., 1998; Stockmeyer and Kruse, 1991; Zhu et al., 2008b). Previous studies have demonstrated that the adsorption capacity of OC is strongly affected by the interlayer surfactant loading amount and structures (Boyd et al., 1988a, 1988b, 1988c; Jaynes and Boyd, 1991a, 1991b). Therefore, many experimental studies have focused on the arrangement and conformation of alkylammonium ions in the interlayer space of clay minerals (He et al., 2004; Kung and Hayes, 1993; Lagaly, 1981, 1986; Lagaly and Weiss, 1969, 1971; Osman et al., 2000, 2002; Tamura and Nakazawa, 1996; Vaia et al., 1994; Xu and Boyd, 1995b; Zhu et al., 2005, 2008a).

So far, X-ray diffraction (XRD) has been widely used to determine the basal spacing of OC. Based on the assumption that all the alkyl chains have *all-trans* conformations, the arrangement of intercalated alkylammonium ions has been proposed in several studies (Lagaly, 1981, 1986; Tamura and Nakazawa, 1996; Yui et al., 2002). The alkyl chains were postulated to orient parallel to the clay mineral surface in monolayer, bilayer, pseudo-trilayer, and then form paraffin-type arrangement. Furthermore, Fourier transform infrared (FTIR) spectroscopy and $^{13}C$ magic angle spinning nuclear magnetic ($^{13}C$ MAS NMR) have been used to probe the conformation and phase state of intercalated alkylammonium ions in layered clay minerals by monitoring the frequency shifts of methylene on alkyl chains (Osman et al., 2000, 2002, 2004; Vaia et al., 1994; Wang et al., 2000; Zhu et al., 2005, 2008a). These studies showed that there is an extensive coexistence of *gauche* and *all-trans* conformations for the alkyl chains and the molecular conformations vary from liquid-like to solid-like as the loading level increases. However, the structural and dynamic information of these intercalated alkylammonium ions is still difficult to be experimentally quantified.

Recently, molecular simulations were introduced into the study of the structure of dried OC and proved to be powerful methods in complementing experiments, especially in probing the details about

* Corresponding author. Tel./fax: +86 20 85290755.
*E-mail address:* zhujx@gig.ac.cn (J. Zhu).

http://dx.doi.org/10.1016/j.clay.2014.05.029
0169-1317/

molecular arrangements and conformations at the atomic level (Greenwell et al., 2005; Hackett et al., 1998; He et al., 2005; Heinz et al., 2003, 2005, 2007; Liu et al., 2007; Tambach et al., 2006; Zeng and Yu, 2008; Zeng et al., 2003, 2004). Layered arrangements of alkylammonium chains in the interlayer space of montmorillonite (Mt) have been discovered in several studies (Heinz et al., 2003, 2005, 2007; Zeng and Yu, 2008; Zeng et al., 2004). Furthermore, the conformation of alkyl chains has been studied in detail and different distribution of *gauche-trans* conformations with respect to basal spacing has been revealed (Heinz et al., 2007; Tambach et al., 2006). These simulations reproduced XRD measurements and revealed the layering configuration of alkyl chains. Nevertheless, the abovementioned structures of interlayer organic phases obtained from dry models of OC may be different in wet state.

It is essential to study the exact interlayer structure of wet organo-montmorillonite (OMt) for better understanding the adsorption process. Previous FTIR studies showed that water molecules have evident influence on the arrangement of alkyl chains on the silica surface, changing it from layered structure to aggregated clusters (Kung and Hayes, 1993). Xu and Boyd pointed out the structures deduced from dried OMt did not represent those in the water saturated condition (Xu and Boyd, 1995a). Based on the change of basal spacing, they suggested loose and probably less ordered arrangements of surfactant in the interlayer space of wet sample. Zhu et al. (2008a) carried out the *in situ* structural characterization of OC in the water saturated condition using XRD and FTIR. The results showed that the structure and properties of intercalates were restricted by surfactant loading and differed from the configuration in the dry OMt. These studies of wet OMt samples proposed several models of surfactant arrangements within the interlayer spaces, but the details about the arrangement and orientation of the surfactant molecules remain ambiguous.

In this paper, the structure and dynamics of water saturated OMt at the atomic level were studied by employing molecular dynamic (MD) simulations. Considering the influence of layer-charge density and surfactant loading amount, two Mt models with different CEC and different loading levels were built on the basis of previous experimental studies. Then, the structural and dynamic properties of the systems in the water saturated condition were systematically investigated. The arrangement, conformation, bonding behavior and dynamics of alkyl ammoniums in the interlayer spaces are uncovered and the effects of water molecules are addressed in detail.

## 2. Methods

### 2.1. Models

Two Mt models with distinctly different layer-charge amount were selected in this study to investigate the influence of Mt layer charge. One with a cation exchange capacity (CEC) of 106 mequiv/100 g is obtained from Inner Mongolia, China (abbreviated M-Mt) on the basis of previous experimental study (Zhu et al., 2008a). The other Mt model with a larger CEC of 131 mequiv/100 g is the Arizona-type Mt (abbreviated A-Mt) (Tambach et al., 2004). The chemical composition of the corresponding Mt models can be expressed as $X_{0.75}[Al_{3.25}\ Mg_{0.75}][Si_8]O_{20}(OH)_4$ and $X[Al_3Mg][Si_8]O_{20}(OH)_4$, respectively where $X$ represents monovalence interlayer compensator cations. In these Mt models, the isomorphic substitutions obey Loewenstein's rule (Loewenstein, 1954). The simulation cell consists of two layers of 32 unit cells each: 8 in x-dimension and 4 in y-dimension, i.e. $8 \times 4 \times 2$ super cell. The surfactant used in this study was cetyltrimethylammonium ($CTMA^+$) for comparison with the experimental studies (Zhu et al., 2008a). For each Mt model, eight different surfactant loading levels from 0.25 CEC to 2.0 CEC were selected, representing systems from incomplete cation exchange to excessive surfactant loading based on experimental results (Zhu et al., 2008a). In 1.0 CEC models, interlayer cations were fully replaced by $CTMA^+$. In the models that loading level unequal to CEC, $Ca^{2+}$ and $Br^-$ ions were added in the interlayer space to balance the charge due to the experimental data (Zhu et al., 2008a). It is hard to obtain exact water content through the mass of water because of the lack of TGA (thermal gravimetry analysis) data in wet samples. Here water contents were first roughly estimated water contents by the equation below:

$$N_{\text{water}} = \frac{V_{\text{water}} \times \rho_{\text{water}}}{M_{\text{water}}} \times N_{\text{a}} \quad (1)$$

Here $N_{\text{water}}$ is the total number of water molecules. $V_{\text{water}}$ is the volume of water molecules in the interlayer space of the Mt models. It is calculated on the basis of the basal spacings of wet OMt samples (Zhu et al., 2008a). $\rho_{\text{water}}$ is the density of water in the interlayer space of Mt. Previous MC and MD simulations showed that the density of water in natural hydrated Na + Mt with basal spacing of 1.5 nm was 1.14 g/cm$^3$, whereas 0.985 g/cm$^3$ in Mt nanopore of 4.5 nm (Botan et al., 2011; Skipper et al., 1991), indicating that water density is closely related to the size of Mt nanopores. Therefore, as a compromise, density of liquid water is used as $\rho_{\text{water}}$ in this study. $M_{\text{water}}$ and $N_{\text{a}}$ correspond to formula mass and the Avogadro constant respectively. Then, NPT ensemble simulations were performed to test the basal spacing and water molecules were added or reduced to obtain a simulation basal spacing close to the value from XRD characterization (Zhu et al., 2008a). For each model, 20 water molecules were added or reduced at each test step. Finally the exact water contents for M-Mt were found. For Arizona Mt model (A-Mt), because of lack of experimental data, the exact water content in the interlayer space is hard to determine. Considering that the water content for M-Mt has been determined from wet samples of experiment, the same water contents were applied to approximately achieve the water saturated condition. Table 1 showed the contents of interlayer species with different surfactant loading levels. All the ions and molecules were placed randomly in the center of Mt interlayer space as initial configuration. For clarity, the denotations of all models were defined by combining Mt types and surfactant loading levels. For example, M-Mt-0.25 represents the system of M-Mt and 0.25 CEC loading level.

### 2.2. Simulation details

CLAYFF was used to describe interatomic potentials for the Mt, calcium ions and water components as it is superior in addressing the effects of different substitutions (Cygan et al., 2004b). CLAYFF was developed specifically for clay minerals and has been widely used successfully to study the clay mineral–water interface (Du and Miller, 2007; Greathouse and Cygan, 2006; Zeitler et al., 2012; Zhu et al., 2013). $CTMA^+$ and $Br^-$ were represented by CVFF model which can be integrated with CLAYFF because of the same Lennard–Jones 12–6 potential form (Dauberosguthorpe et al., 1988). The combined force field has been successfully used in the simulations of mineral-organic interfaces and alkylammonium intercalated Mt (Cygan et al., 2004a; Liu et al.,

**Table 1**
Interlayer ions and water contents of simulation systems.

| Loading levels | M-Mt | | | | A-Mt | | | |
|---|---|---|---|---|---|---|---|---|
| | $CTMA^+$ | $Ca^{2+}$ | $Br^-$ | $H_2O$ | $CTMA^+$ | $Ca^{2+}$ | $Br^-$ | $H_2O$ |
| 0.25 CEC | 12 | 18 | 0 | 814 | 16 | 24 | 0 | 814 |
| 0.50 CEC | 24 | 12 | 0 | 1600 | 32 | 16 | 0 | 1600 |
| 0.75 CEC | 36 | 6 | 0 | 1344 | 48 | 8 | 0 | 1344 |
| 1.00 CEC | 48 | 0 | 0 | 1200 | 64 | 0 | 0 | 1200 |
| 1.25 CEC | 60 | 0 | 12 | 1242 | 80 | 0 | 16 | 1242 |
| 1.50 CEC | 72 | 0 | 24 | 1200 | 96 | 0 | 32 | 1200 |
| 1.75 CEC | 84 | 0 | 36 | 1177 | 112 | 0 | 48 | 1177 |
| 2.00 CEC | 96 | 0 | 48 | 1006 | 128 | 0 | 64 | 1006 |

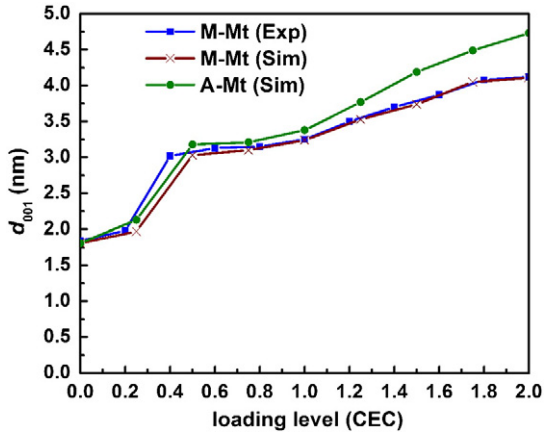


**Fig. 1.** Calculated and experimental basal spacing for $CTMA^+$ intercalated Mt as a function of surfactant loading level.

2009, 2010, 2011). As an empirical potential, CLAYFF and CVFF have limitations. CLAYFF overestimates the surface energy, whereas INTERFACE, another successful force field for clay–organic systems reproduces better interfacial energies (Heinz et al., 2013). CVFF contains a stronger torsion barriers in alkyl chains comparing to PCFF (Sun, 1995), which may lead to a smaller percentage of gauche conformation. In this study, these limitations do not affect the qualitative conclusions.

In CLAYFF-CVFF, the total energy of the OMt is calculated as (Cygan et al., 2004b):

$$E_{total} = E_{Coul} + E_{VDW} + E_{bondstretch} + E_{anglebend} + E_{torsion} \quad (2)$$

Here $E_{total}$, $E_{Coul}$, $E_{VDW}$, $E_{bondstretch}$, $E_{anglebend}$ and $E_{torsion}$ denote the coulombic interaction, the Van der Waals interaction, the bond stretching, the bond bending and the torsion terms, respectively. The first three terms are calculated to represent the energy of the Mt framework based on CLAYFF, and all terms are evaluated for the intercalated ions based on CVFF. A 15.0 Å cut-off was used for the short-range interactions. The coulombic interaction was treated using the Ewald summation and the number of k-space vectors was determined to reach a precision of $1.0 \times 10^{-4}$. Three dimensional periodic boundary conditions were selected during the simulations.

All MD simulations were undertaken using DL_POLY (version 2.20) (Smith and Forester, 1996). Geometry optimizations were used to get a minimum energy structure. Then, NPT (298 K, 1 atm) simulations were performed to achieve equilibrium for 2000 ps, and another 500 ps to record the results. When systems reach equilibrium, a further 500 ps NVT (298 K) simulation was performed following the previous 2500 ps NPT simulation to obtain the interlayer space structures and dynamic properties. In all simulations, the time step was set to be 1.0 fs and all atoms were allowed to move.

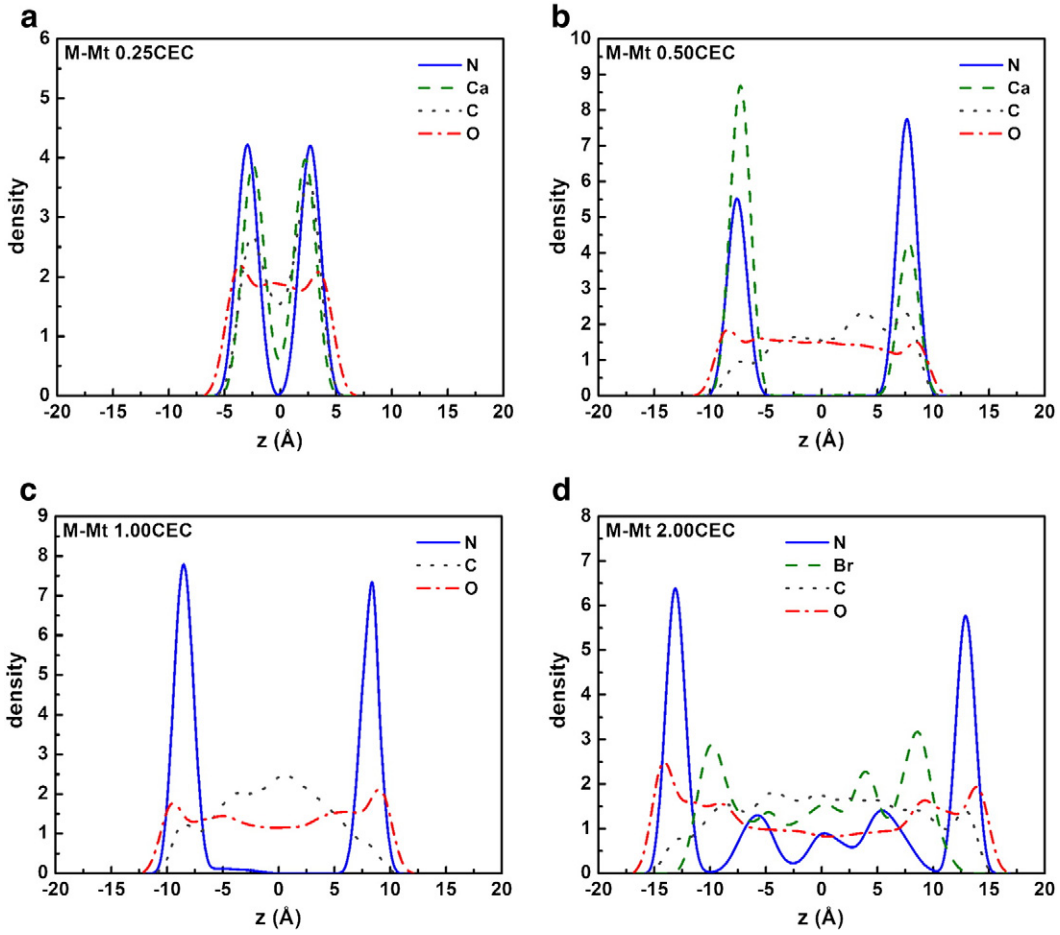


**Fig. 2.** Density distributions of $CTMA^+$ intercalated Mt. Zero point of the horizontal axis denotes the center of z axis of each system. (a) M-Mt-0.25; (b) M-Mt-0.50; (c) M-Mt-1.00; (d) M-Mt-2.00; (e) A-Mt-0.25; (f) A-Mt-0.50; (g) A-Mt-1.00; (h) A-Mt-2.00.

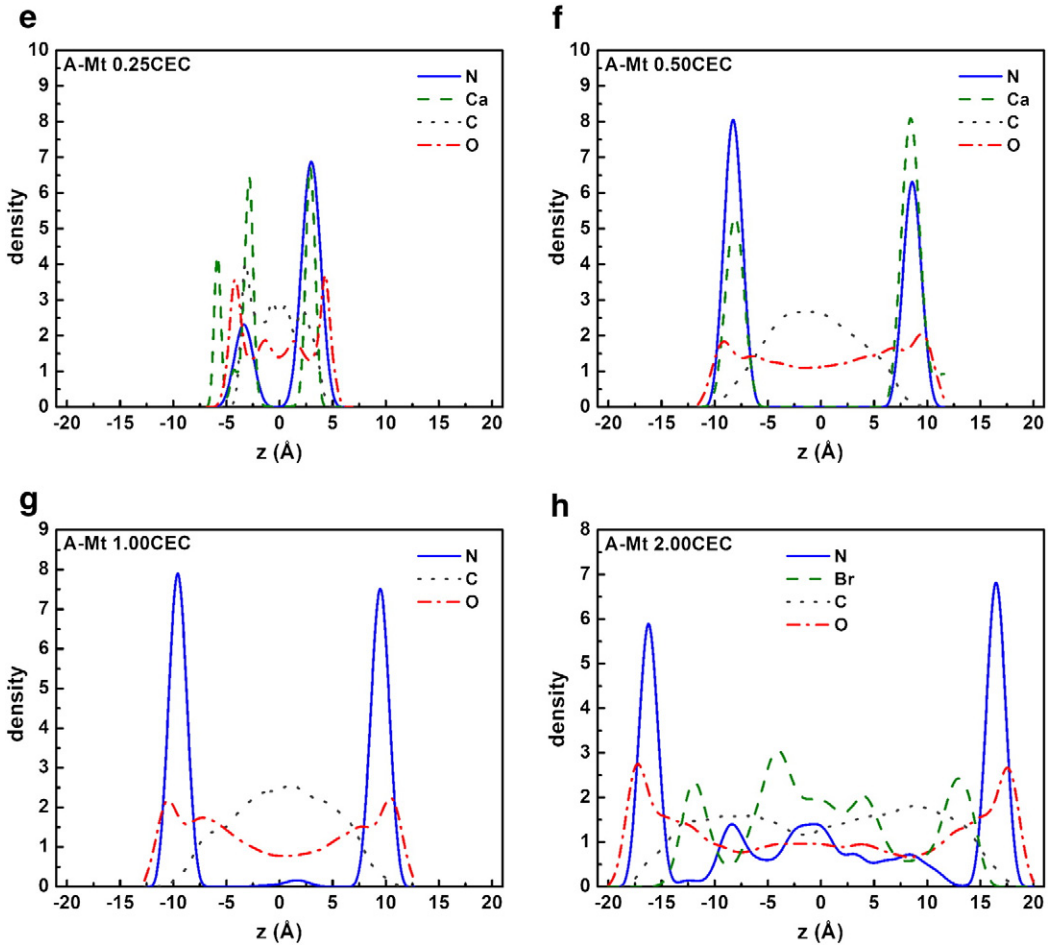


**Fig. 2** (*continued*).

## 3. Results and discussions

### 3.1. Basal spacing and density distributions

The basal spacings of the experimental and simulated water saturated OMt systems represent a stepwise behavior (Fig. 1). The basal spacings of M-Mt models are consistent with the results from XRD characterization (Zhu et al., 2008a). The basal spacings of A-Mt models are slightly higher than the corresponding M-Mt models at low surfactant loading, but the disparity increases as the loading level increases. It can be seen that the adsorption of alkylammonium and water in the interlayer spaces can enlarge the basal spacing.

The density distributions for ammonium N, alkyl C, $Ca^{2+}$, $Br^{-}$ and water O changes in both M-Mt and A-Mt with different surfactant loading level (Fig. 2), as shown in visualized snapshots of $CTMA^{+}$ intercalated M-Mt (Fig. 3). In M-Mt-0.25 system, both ammonium N and alkyl C are arranged in two layers according to the two clear peaks of the density distributions, indicating a bilayer structure (Fig. 2a). As the surfactant loading level increases, the density distribution of ammonium N remains two peaks close to the silicate surface (Fig. 2b and c), implying the strong electrostatic interaction between negative charge site and ammonium N. In contrast, the distribution of alkyl C transforms to one broad peak (Fig. 2c) in the center, indicating a surfactant aggregation forms in the interlayer space and the arrangement of alkyl chains is inclined to the Mt surface (Fig. 3b and c). $Ca^{2+}$ displays a symmetrical distribution with ammonium N to balance negative charge site in the incomplete cation exchange cases. In the excessive surfactant loading cases (Fig. 2d), the small peaks of ammonium N in the interlayer space are in accordance with $Br^{-}$, representing the $CTMA^{+}$ and $Br^{-}$ ion pairs in the center of interlayer space (Fig. 3d). The result is different from the monolayer, bilayer and pseudo-trilayer models as surfactant loading increases for dry samples (Lagaly, 1981, 1986; Lagaly and Dekany, 2005; Lagaly and Weiss, 1971; Zeng et al., 2003, 2004). In the center of the interlayer space, the alkyl chains are connected closely and clearly reflect the hydrophobic interactions between the alkyl chains (Fig. 3). In all cases, the density of water near the Mt surface is higher, which can be attributed to the combined effects of hydrophilic Mt surface and ammonium head groups.

The density distributions of interlayer species for A-Mt in most cases show the similar phenomena as those for M-Mt (Fig. 2f–h). However, in A-Mt-0.25 system, the alkyl C forms several peaks near the center of the interlayer space (Fig. 2e) instead of two peaks in M-Mt-0.25 system (Fig. 2a). The fluctuating distributions of alkyl chains indicate that the arrangement of $CTMA^{+}$ is probably dependent on the surfactant loading amount in the interlayer space of Mt affected by CEC. To sum up, under the water saturated condition, alkyl chains are likely to concentrate in the center of the Mt interlayer space, which is consistent with experimental results (Zhu et al., 2008a).

### 3.2. Orientation of alkyl chains

Although the density distribution has revealed the alignment of interlayer species, the orientation of integral $CTMA^{+}$ in the interlayer space of Mt remains unknown. Early experimental researches used tilt angle of the alkyl chain with respect to the silicate surface to describe the arrangement of idealized *all-trans* structures of alkyl ammonium (Bergaya et al., 2006; Lagaly, 1981, 1986; Lagaly

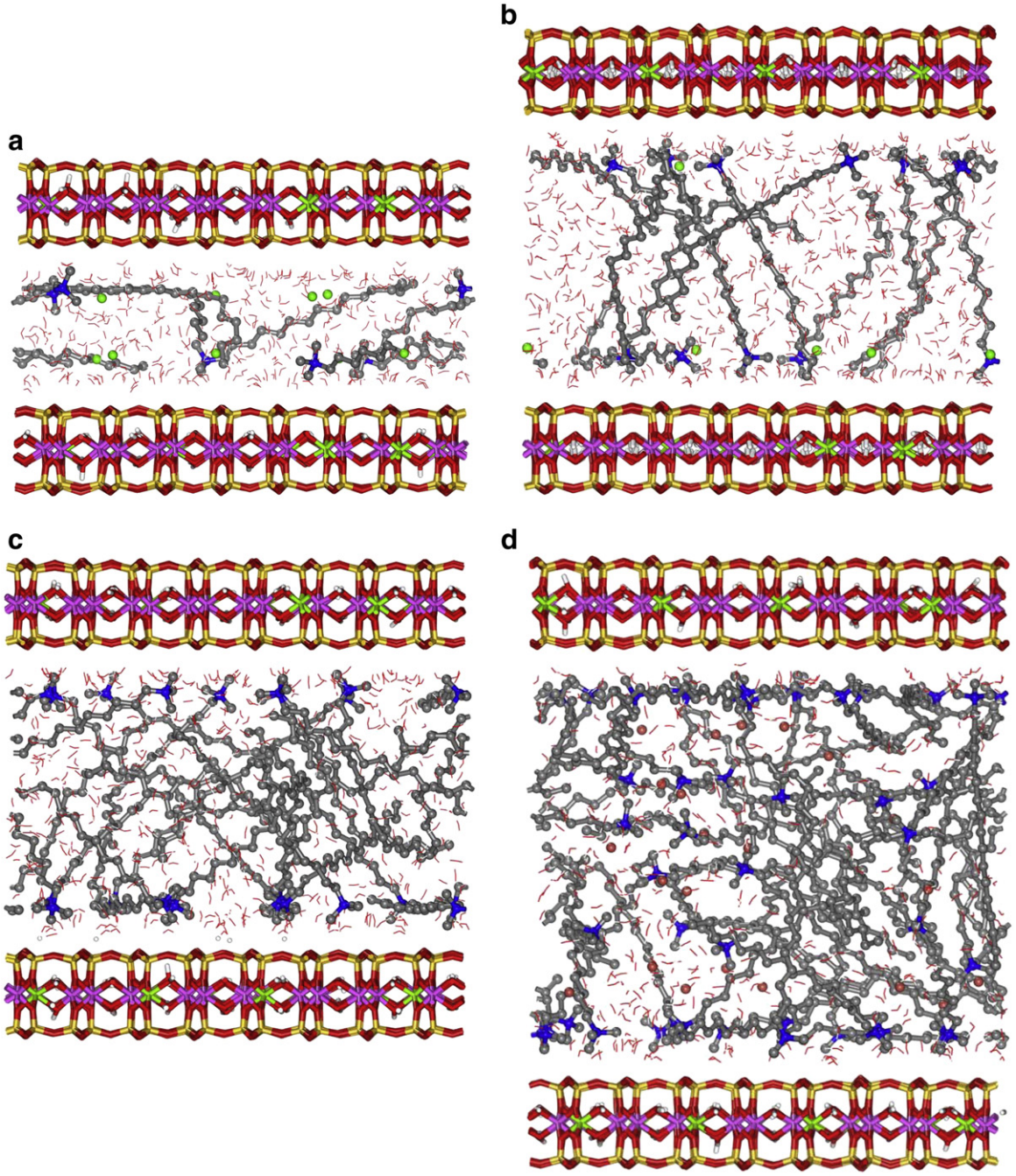


**Fig. 3.** Snapshots of $CTMA^+$ intercalated M-Mt. In each snapshot, the stick layer represents the Mt layers. For the atoms in the interlayer space, Ca = Green, N = blue, C = grey, Br = Brown, H = white, O = red. (a) 0.25 CEC; (b) 0.50 CEC; (c) 1.00 CEC; (d) 2.00 CEC.

and Weiss, 1969). However, recent experimental and simulation researches both reveal that *all-trans* conformation rarely exists in the whole long alkyl chains (He et al., 2004; Heinz et al., 2003, 2007; Osman et al., 2002; Vaia et al., 1994; Zeng et al., 2003; Zhu et al., 2005, 2008a). Here it is considered that tilt angle as the statistic value of different segments along the alkyl chains to obtain

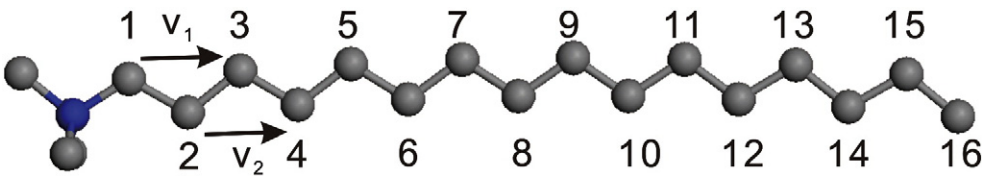


**Fig. 4.** Schematic of the $CTMA^+$ chain. Hydrogen atoms are removed for clarity. The numbers of carbon atoms along alkyl chain backbone are given. The vectors (v) connecting two $CH_2$ segments separated by two bonds used in the tilt angle analysis are indicated. For instance, $v_1$ corresponds to vectors between carbon number 1 and 3.

quantitative information on the orientation of the individual molecule and spatial distribution. Therefore, on the basis of previous researches (Adolf et al., 1995; Smith et al., 1999; Zeng and Yu, 2008; Zeng et al., 2004), the tilt angle is defined as the angle between a unit vector perpendicular to the silicate surface and a vector connecting two methylene separated by two bonds along the alkyl chain (Fig. 4). The tilt angle ranges from zero to 90°. A zero tilt angle represents a radiating arrangement that the segment is normal to the surface, while a 90° tilt angle corresponds to a layered structure that the segment is parallel with the surface. The tilt angles are averaged on all segments of alkyl chains over the NVT stage.

The average tilt angle is around 80° in M-Mt-0.25 system and 70° in A-Mt-0.25 system, which indicates that the chains are parallel with the surface (Fig. 5a). Moreover, the tilt angles of vectors close to ammonium head groups are lower than those on the tail, revealing that the tails of alkyl chains are more likely to orient parallel to the clay mineral surface within a limited interlayer space. The average tilt angle falls down to 55° as the surfactant loading level increases, showing that the alkyl chains tend to radiate away from the Mt surface (Fig. 5b) which agrees well with the density distribution. In 1.00 CEC cases (Fig. 5c), contrary to the 0.25 CEC cases, there is a step downward between carbon atom 5 and 6 which indicates the tails of alkyl chain are less likely to be parallel to the surface with paraffin-type arrangement. In 2.00 CEC cases (Fig. 5d), the step disappears and the average tilt angle of all segments along alkyl chains is 55°.

The tilt angles of segments of alkyl chains with respect to the z direction show the arrangement of $CTMA^+$ in the interlayer space (Fig. 6). In 0.25 CEC cases, the clear bilayer structure of alkyl chains can be found (Fig. 6a). From 0.50 CEC to 2.00 CEC cases, the tilt angle of segments near silicate surface is about 80°, indicating that part of the alkyl chains are still parallel with the surface through intermolecular interaction (Fig. 6b–d). On the other hand, the tilt angles of segments in the center of interlayer space fluctuate between 45° and 60°, which is consistent with the result of density distributions that $CTMA^+$ in the interlayer space form paraffin alignment other than layered configuration. Compared to the average tilt angle in the interlayer space of dried OMt (70°) (Zeng et al., 2003), the tilt angles in wet systems are smaller, showing that alkyl chains are less layered than dry system. This further confirms that water molecules enlarge the interlayer space of OMt and reduce the interaction between alkyl chains and silicate surface. Therefore, in the water saturated systems, the arrangement of surfactant is different from the traditional layered configurations as shown in dry systems. The alkyl chains form an inclined paraffin-type arrangement with average tilt angle of 35° with the surface (Liu et al., 2007; Tambach et al., 2006; Zeng et al., 2003, 2004). This arrangement turns the interlayer space environment into a more hydrophobic medium which contributes to the adsorption of organic contaminants, corresponding to experimental studies (Zhu et al., 2008a). The tilt angles relative to the surface increase as the surfactant loading level increases in both M-Mt and A-Mt systems, which is consistent with previous findings in dry systems (Heinz et al., 2008). This implies whether in the

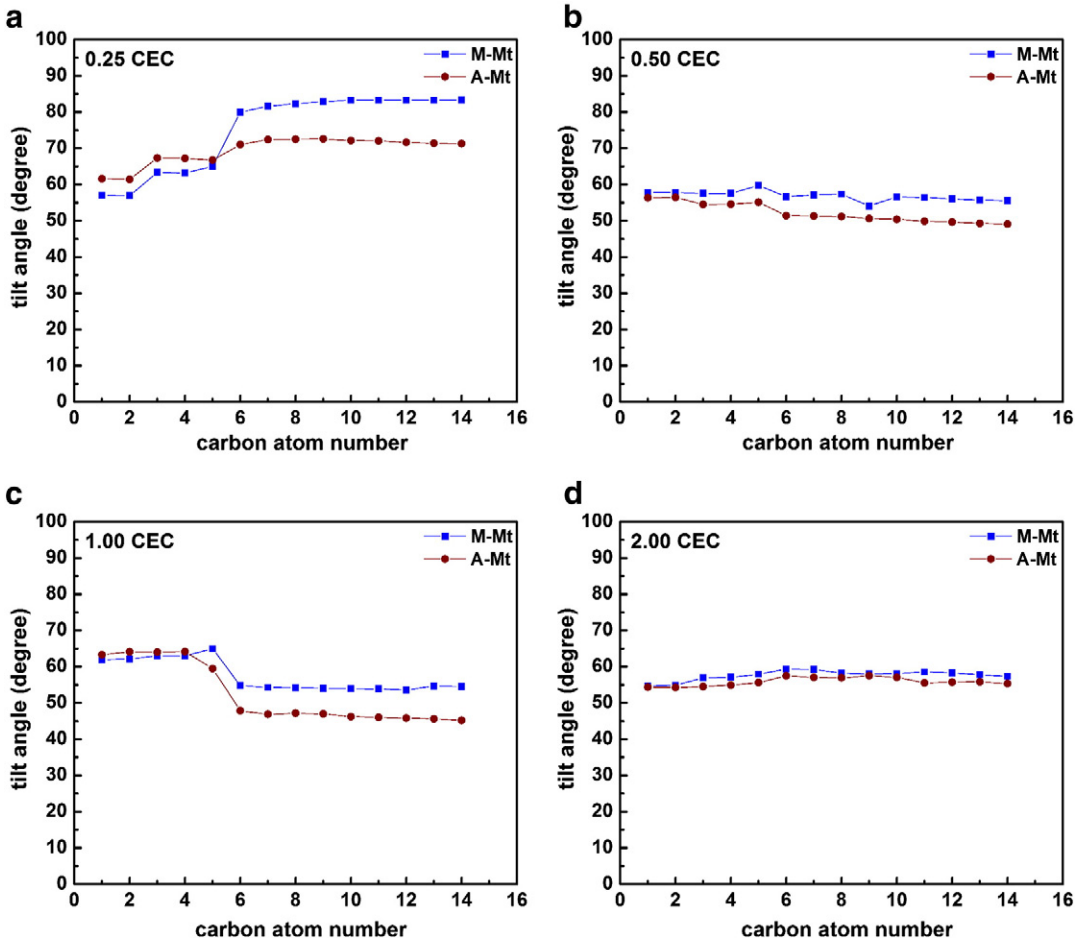


**Fig. 5.** Tilt angle distribution of alkyl chains in the $CTMA^+$ intercalated Mt of different loading level as a function of carbon atom number. (a) 0.25 CEC; (b) 0.50 CEC; (c) 1.00 CEC; (d) 2.00 CEC.

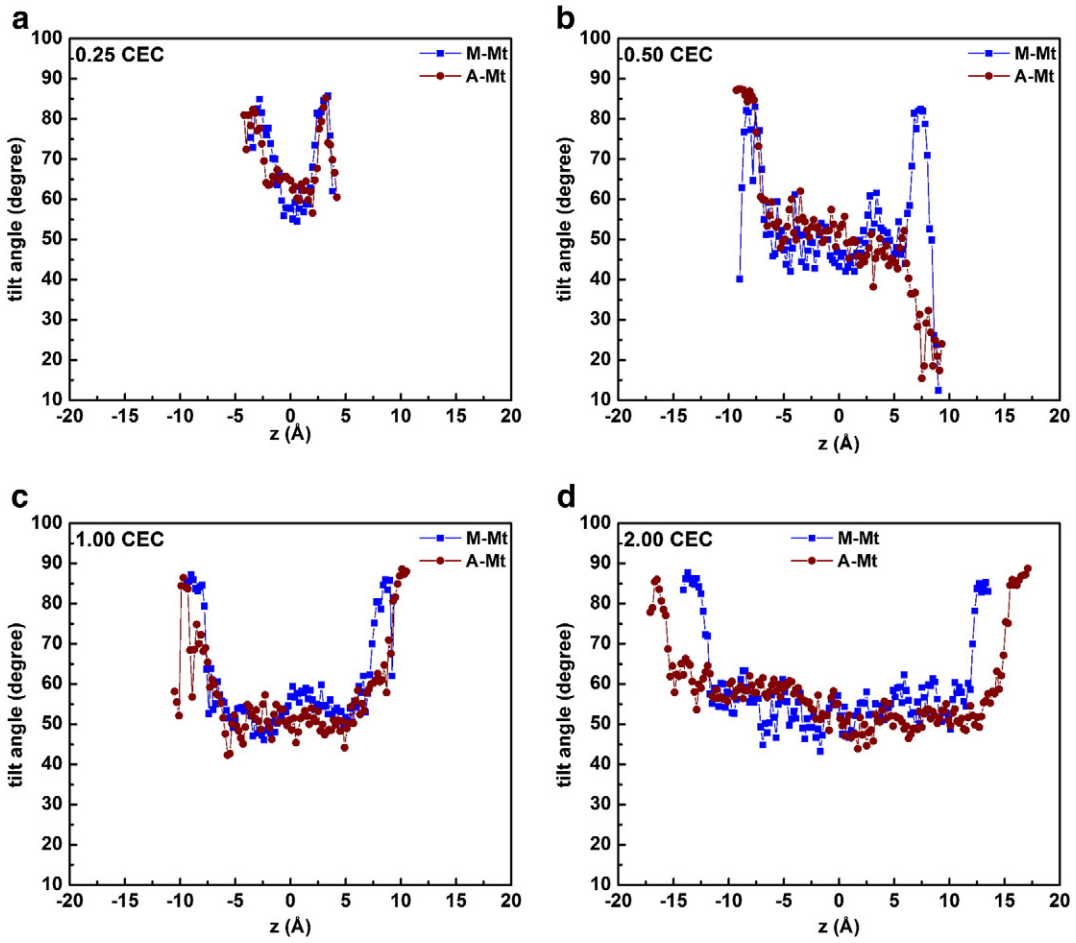


**Fig. 6.** Tilt angle distribution of alkyl chains in the $CTMA^+$ intercalated Mt of different loading level as a function of z distance. (a) 0.25 CEC; (b) 0.50 CEC; (c) 1.00 CEC; (d) 2.00 CEC.

dry or wet systems, surfactant arrangement changes from layered to inclined paraffin with increasing tilt angle with respect to the surface.

### 3.3. Conformation of alkyl chains

The fractions of *gauche* conformations of alkyl chains are calculated from the total number of torsional dihedral angles along the N-$C_n$ backbone. In each model, averaging in the conformational analysis is performed over all $CTMA^+$ in 500 snapshots of NVT stage (Heinz et al., 2007). As shown in Fig. 7, the *gauche* conformation of the alkyl chains of $CTMA^+$ in both M-Mt and A-Mt varies from 12% to 19% as a function of loading level. The average fraction of *gauche* conformations at normal temperature is found to be between the value in a hydrocarbon crystal (about 5% *gauche* conformation) and those in liquid alkanes (about 25% *gauche* conformation) (Vaia et al., 1994). Compared to previous simulations of dried OMt (15–25% *gauche* conformations of $CTMA^+$ at 1.00 CEC) (Heinz et al., 2007; Tambach et al., 2006), our results show a more ordered conformation, which are consistent with the experimental conclusions (Kung and Hayes, 1993). It can be explained that water molecules enlarge the interlayer space and make alkyl chains easier to stretch to *all-trans* conformation. For the M-Mt models, the percentage of *gauche* conformation increases to a maximum at 0.75 CEC at first. Then, it decreases gradually as surfactant loading level increases until 1.75 CEC. In A-Mt models, similar to M-Mt, the percentage of *gauche* conformation increases gradually and reaches a summit at 1.00 CEC. In the excessive surfactant loading cases, the percentages of *gauche* conformation decrease at 1.25 CEC and fluctuate from 1.25 CEC to 2.00 CEC.

FTIR studies of water saturated $CTMA^+$ intercalated Mt indicated that the surfactant intercalates have a more ordered phase at high surfactant packing density (Zhu et al., 2008a). Here it is observed that the occurrence of *gauche* conformations in the system is related to the surfactant loading level in the water saturated systems. The alkyl ammoniums are likely to form more ordered conformations (less *gauche*) at both low and high surfactant loading levels. In the cases of very low loading level (i.e. 0.25 CEC), $CTMA^+$ formed bilayer structures and the alkyl chains have orientations parallel to the silicate surface (Figs. 2a

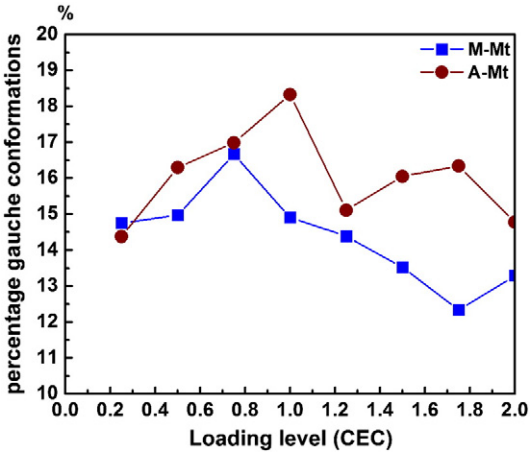


**Fig. 7.** Conformations in the alkylammonium molecules as a function of surfactant loading level for M-Mt and A-Mt.

and 6a). The alkyl chains have a smaller percentage of *gauche* conformations with layered configuration due to confinement, which is consistent with previous simulation of dry OMt (Tambach et al., 2006). This also indicates that a small quantity of water scarcely affects the alkyl chain configuration at very low loading levels. As the loading level increases to 1.00 CEC, the basal spacing of $CTMA^+$ intercalated Mt increases and the alkyl chains prefer the arrangement radiating away from the surface. In these cases, alkyl chains are more favorable to entangle with each other due to weaker confinement of the silicate surface, resulting in more disordered conformations. In the excessive surfactant loading cases, more $CTMA^+$ were adsorbed into the interlayer spaces with $Br^-$ by the attraction between the hydrophobic alkyl chains while the basal spacing did not increase observably. The fraction of disordered conformation decreases due to the steric hindrance of molecular surfactant, which is consistent with FTIR results (Zhu et al., 2008a). Besides, the fluctuation in both M-Mt and A-Mt models at high loading level shows the influence of water molecules. In these cases (i.e. M-Mt-2.00, A-Mt-1.50 and A-Mt-1.75), the fraction of *gauche* conformation does not decrease as loading level increases, indicating that water adds the randomness to the percentage of disordered conformation.

### 3.4. Interlayer bonding behavior

The bonding behaviors of the interlayer species in the OMt can be explored based on their radial distribution functions (RDF) and coordination numbers (CN). Fig. 8 illustrates the curves of the RDF for surface O of clay mineral layer (Oc) around ammonium N (Fig. 8a), water O (Ow) around ammonium N (Fig. 8b), water H (Hw) around surface O (Oc) (Fig. 8c) and $Br^-$ around ammonium N (Fig. 8d) in the M-Mt model. Two main N-Oc pair correlation peaks near 4.8 Å and 7.9 Å are formed in all cases (Fig. 8a). The average CN of N-Oc at all loading levels are about 6, indicating that ammonium N all locate above the surface six-member rings and coordinate with surface O. The RDF for water oxygen atoms (Ow) around ammonium N at all loading level show a sharp peak near 4.8 Å and a broad peak near 7.5 Å (Fig. 8b), suggesting a strong N–Ow pair correlation and a second hydration shell. The CN of N–Ow calculated from the RDF range from 4 to 6. These results indicate that in the water saturated condition, ammonium N are firmly fixed above the center of the hexagonal ring of Mt surface and partly covered by water molecules (Zhou et al., 2011). The RDF between water H and surface O in M-Mt present two clear peaks: one centered at 2.0 Å and the other at 3.5 Å (Fig. 8c), which indicate strong interactions between water H and surface O. Fig. 8d illustrates the RDF for $Br^-$ around ammonium N for the excessive surfactant loading cases. The sharp peak in the RDF curves shows a strong correlation between $Br^-$ and ammonium N due to the electrostatic interactions. The RDF features of A-Mt models are nearly the same as those for M-Mt and detail information can be found in supporting information.

### 3.5. Dynamic of interlayer species

Dynamic properties from MD simulations provide useful information about the mobility of interlayer $CTMA^+$ in the water saturated condition. The self-diffusion coefficients of ammonium N and alkyl C in the interlayer space of M-Mt-1.00 system are $1.47 \times 10^{-11}$ $m^2/s$ and $2.02 \times 10^{-11}$ $m^2/s$ (Table 2), which are much lower than the water molecules ($156 \times 10^{-11}$ $m^2/s$). The low mobility of the

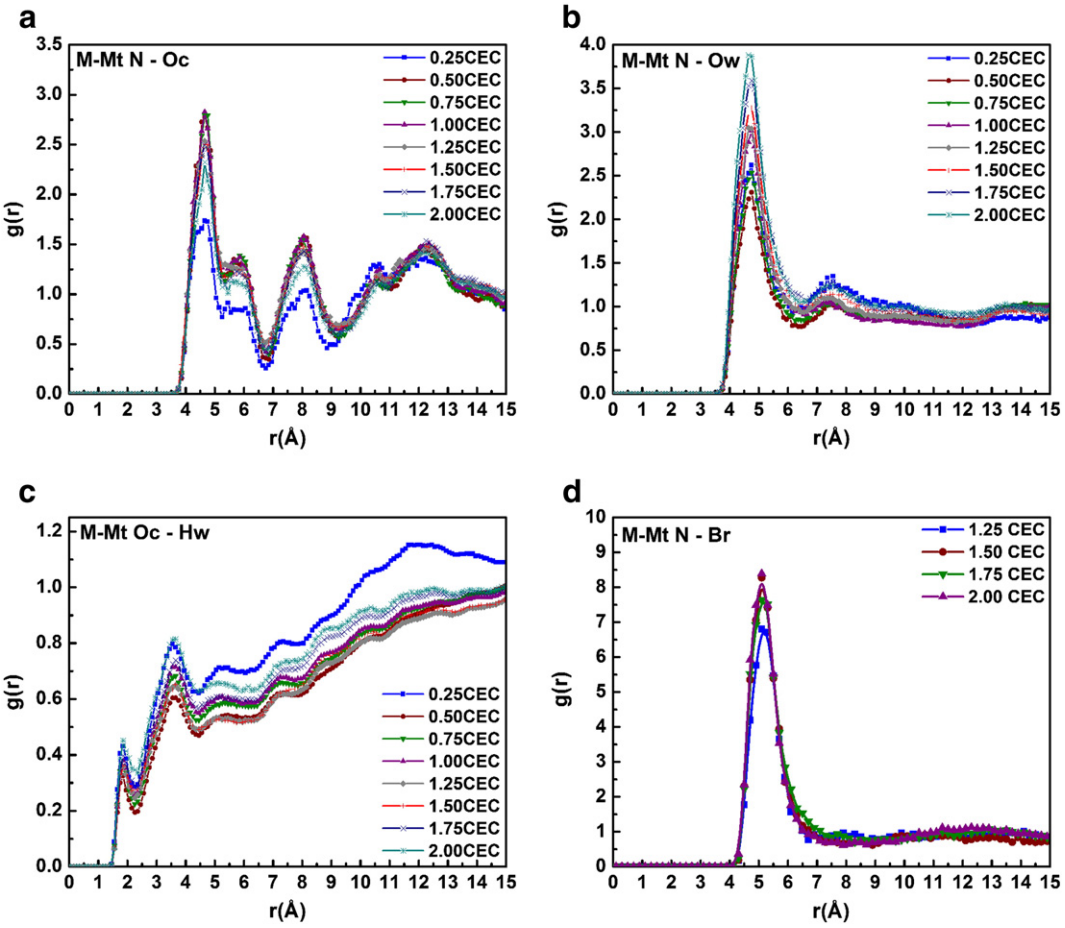


**Fig. 8.** Radial distribution functions: (a) surface oxygen around $CTMA^+$ N in M-Mt (b) water oxygen around $CTMA^+$ N in M-Mt; (c) water hydrogen around surface oxygen in M-Mt (d) bromine ions around $CTMA^+$ in M-Mt.

**Table 2**
Self-diffusion coefficients for interlayer species ($10^{-11}$ $m^2/s$).

| Loading levels | M-Mt | | | | | A-Mt | | | | |
|---|---|---|---|---|---|---|---|---|---|---|
| | N | C | Ow | $Ca^{2+}$ | $Br^-$ | N | C | Ow | $Ca^{2+}$ | $Br^-$ |
| 0.25 CEC | 2.01 | 3.45 | 114.04 | 5.78 | – | 0.72 | 1.14 | 92.13 | 2.02 | – |
| 0.50 CEC | 2.37 | 3.87 | 168.02 | 3.87 | – | 1.16 | 2.40 | 149.23 | 4.06 | – |
| 0.75 CEC | 1.45 | 1.77 | 161.42 | 3.57 | – | 1.02 | 0.95 | 114.29 | 3.15 | – |
| 1.00 CEC | 1.47 | 2.02 | 155.98 | – | – | 0.65 | 1.40 | 108.27 | – | – |
| 1.25 CEC | 1.89 | 1.72 | 129.38 | – | 11.70 | 1.14 | 1.07 | 86.39 | – | 12.47 |
| 1.50 CEC | 2.61 | 2.28 | 145.67 | – | 15.75 | 1.44 | 1.85 | 95.30 | – | 8.26 |
| 1.75 CEC | 2.90 | 2.85 | 145.61 | – | 16.33 | 1.90 | 1.87 | 68.80 | – | 8.29 |
| 2.00 CEC | 1.78 | 1.99 | 99.06 | – | 7.02 | 1.63 | 1.74 | 59.75 | – | 7.12 |

ammonium N of $CTMA^+$ is in accordance with the density distribution, both of which indicate that most of the ammonium N are closely related to the surface six-member rings. The self-diffusion coefficient of alkyl chains in previous simulation which used dry A-Mt model for 1.00 CEC case is $0.86 \times 10^{-11}$ $m^2/s$ (Liu et al., 2009). Compared to that value, the self-diffusion coefficient for alkyl chain in the interlayer space of A-Mt-1.00 system is higher ($1.40 \times 10^{-11}$ $m^2/s$), indicating that the alkyl chain in the middle of interlayer space undergoes faster motions under the water saturated condition. This suggests that water molecules in the interlayer space may reduce the confining effect of Mt surfaces and increase the mobility of alkyl chains. In addition, the self-diffusion coefficient of water in the interlayer space of OMt for dried sample is $13 \times 10^{-11}$ $m^2/s$ (Liu et al., 2007), while the value is $230 \times 10^{-11}$ $m^2/s$ in bulk condition (Ohtaki and Radnai, 1993). The obtained values in all our simulation systems are between the two values above due to the effect of both water molecules and Mt layers.

In the incomplete cation exchange cases of M-Mt, the self-diffusion coefficients of ammonium N and alkyl C first increase to a maximum at 0.50 CEC, then lower to a minimum at 0.75 CEC. This is because at 0.50 CEC, a large amount of water enters the interlayer space and enlarges the basal spacing, then more $Ca^{2+}$ are replaced by $CTMA^+$. In the excessive surfactant loading cases, the mobility of ammonium N is larger than 1.0 CEC for the reason that part of the ammonium N are not fixed at the Mt surface. Compared with those in M-Mt, the self-diffusion coefficients of all interlayer species in A-Mt are smaller at all surfactant loading levels. Previous researches demonstrate that negatively charged clay mineral layers have confining effects on surface water (Zhou et al., 2011). Hence, higher cation exchange capacity of A-Mt leads to stronger confining effect of silicate surface which lowers the mobility of both $CTMA^+$ and water. In M-Mt-0.50 and A-Mt-0.50 systems, the proportion of water in the interlayer space achieves the maximum. As a result, the self-diffusion coefficient of alkyl chains in these cases is highest, indicating that more water molecule content and larger basal spacing increase the mobility of alkyl chains.

In the incomplete cation exchange cases, the mobility of $Ca^{2+}$ in both M-Mt and A-Mt is low because of not only the strong coulombic interactions with the Mt negative charge site, but also hydration with interlayer water molecules. On the other hand, in the excessive surfactant loading cases, the self-diffusion coefficient of $Br^-$ is higher than ammonium N but lower than water. This is because the electrostatic attractions between $Br^-$ and ammonium N are reduced by the water molecules which coordinate with ammonium N (Fig. 8b).

## 4. Conclusion

Molecular dynamics simulations provide a detailed insight into the structure and dynamic of $CTMA^+$ intercalated Mt in the water saturated condition. The arrangement and conformation of $CTMA^+$ in the interlayer space of wet OMt are affected by water molecules and surfactant loading levels. The configuration of alkyl chains in the water saturated condition changes from bilayer to inclined paraffin-type as the surfactant loading level increases, which is different from dry OMt. Most alkyl chains concentrated in the center of interlayer space with certain orientation, forming hydrophobic organic phase. The conformations of $CTMA^+$ in wet systems show better ordering than those in dry systems. Besides, surfactant loading level also influences the conformation of $CTMA^+$ in wet systems. At low loading level (lower than 0.5 CEC), the confinement of silicate surface induces a more ordered conformation. The percentage of disordered conformation achieves the maximum at 0.75 CEC for M-Mt and 1.00 CEC for A-Mt. At high loading level (exceeding 1 CEC), the steric hindrance of molecular surfactant leads to less *gauche* conformation.

The ammonium head groups locate close to the Mt surface and have correlation with both surface oxygen and water oxygen. They do not present obvious mobility, whereas alkyl chains show a little higher mobility. Water molecules show the highest mobility among the interlayer species. In addition, CEC determines the confining effect of Mt surface which reduces the mobility of both alkyl chains and water molecules.

## Acknowledgments

This research was supported by the grant of the Knowledge Innovation Program of the Chinese Academy of Sciences (KZCX2-EW-QN101), One Hundred Talents Program of the Chinese Academy of Science (KZZD-EW-TZ-10), National Science Foundation of China (Nos. 21177104, 40972034).

## References

Adolf, D.B., Tildesley, D.J., Pinches, M.R.S., Kingdon, J.B., Madden, T., Clark, A., 1995. Molecular-dynamics simulations of dioctadecyldimethylammonium chloride monolayers. Langmuir 11, 237–246.
Bergaya, F., Theng, B.K.G., Lagaly, G., 2006. Handbook of clay science. Elsevier.
Botan, A., Rotenberg, B., Marry, V., Turq, P., Noetinger, B., 2011. Hydrodynamics in clay nanopores. J. Phys. Chem. C 115, 16109–16115.
Boyd, S.A., Lee, J.F., Mortland, M.M., 1988a. Attenuating organic contaminant mobility by soil modification. Nature 333, 345–347.
Boyd, S.A., Mortland, M.M., Chiou, C.T., 1988b. Sorption characteristics of organic-compounds on hexadecyltrimethylammonium-smectite. Soil Sci. Soc. Am. J. 52, 652–657.
Boyd, S.A., Shaobai, S., Lee, J.F., Mortland, M.M., 1988c. Pentachlorophenol sorption by organo-clays. Clays Clay Minerals 36, 125–130.
Cygan, R.T., Guggenheim, S., van Groos, A.F.K., 2004a. Molecular models for the intercalation of methane hydrate complexes in montmorillonite clay. J. Phys. Chem. B 108, 15141–15149.
Cygan, R.T., Liang, J.J., Kalinichev, A.G., 2004b. Molecular models of hydroxide, oxyhydroxide, and clay phases and the development of a general force field. J. Phys. Chem. B 108, 1255–1266.
Dauberosguthorpe, P., Roberts, V.A., Osguthorpe, D.J., Wolff, J., Genest, M., Hagler, A.T., 1988. Structure and energetics of ligand-binding to proteins – escherichia-coli dihydrofolate reductase trimethoprim, a drug-receptor system. Proteins Struct. Funct. Genet. 4, 31–47.
Du, H., Miller, J.D., 2007. Adsorption states of amphipatic solutes at the surface of naturally hydrophobic minerals: a molecular dynamic simulation study. Langmuir 23, 11587–11596.
Greathouse, J.A., Cygan, R.T., 2006. Water structure and aqueous uranyl(VI) adsorption equilibria onto external surfaces of beidellite, montmorillonite, and pyrophyllite: results from molecular simulations. Environ. Sci. Technol. 40, 3865–3871.
Greenwell, H.C., Harvey, M.J., Boulet, P., Bowden, A.A., Coveney, P.V., Whiting, A., 2005. Interlayer structure and bonding in nonswelling primary amine intercalated clays. Macromolecules 38, 6189–6200.
Hackett, E., Manias, E., Giannelis, E.P., 1998. Molecular dynamics simulations of organically modified layered silicates. J. Chem. Phys. 108, 7410–7415.
He, H.P., Frost, R.L., Deng, F., Zhu, J.X., Wen, X.Y., Yuan, P., 2004. Conformation of surfactant molecules in the interlayer of montmorillonite studied by C-13 MAS NMR. Clays Clay Minerals 52, 350–356.
He, H.P., Galy, J., Gerard, J.F., 2005. Molecular simulation of the interlayer structure and the mobility of alkyl chains in HDTMA(+)/montmorillonite hybrids. J. Phys. Chem. B 109, 13301–13306.
Heinz, H., Castelijns, H.J., Suter, U.W., 2003. Structure and phase transitions of alkyl chains on mica. J. Am. Chem. Soc. 125, 9500–9510.
Heinz, H., Koerner, H., Anderson, K.L., Vaia, R.A., Farmer, B.L., 2005. Force field for mica-type silicates and dynamics of octadecylammonium chains grafted to montmorillonite. Chem. Mater. 17, 5658–5669.
Heinz, H., Vaia, R.A., Krishnamoorti, R., Farmer, B.L., 2007. Self-assembly of alkylammonium chains on montmorillonite: effect of chain length, head group structure, and cation exchange capacity. Chem. Mater. 19, 59–68.
Heinz, H., Vaia, R.A., Farmer, B.L., 2008. Relation between packing density and thermal transitions of alkyl chains on layered silicate and metal surfaces. Langmuir 24, 3727–3733.

Heinz, H., Lin, T.J., Mishra, R.K., Emami, F.S., 2013. Thermodynamically consistent for the assembly of inorganic, organic, and biological nanostructures: The INTERFACE Force Field. Langmuir 29, 1754–1765.
Jaynes, W.F., Boyd, S.A., 1991a. Clay mineral type and organic-compound sorption by hexadecyltrimethlyammonium-exchanged clays. Soil Sci. Soc. Am. J. 55, 43–48.
Jaynes, W.F., Boyd, S.A., 1991b. Hydrophobicity of siloxane surfaces in smectites as revealed by aromatic hydrocarbon adsorption from water. Clays Clay Minerals 39, 428–436.
Kung, K.H.S., Hayes, K.F., 1993. Fourier-transform infrared spectroscopic study of the adsorption of cetyltrimethylammonium bromide and cetylpyridinium chloride on silica. Langmuir 9, 263–267.
Lagaly, G., 1981. Characterization of clays by organic-compounds. Clay Miner. 16, 1–21.
Lagaly, G., 1986. Interaction of alkylamines with different types of layered compounds. Solid State Ionics 22, 43–51.
Lagaly, G., Dekany, I., 2005. Adsorption on hydrophobized surfaces: clusters and self-organization. Adv. Colloid Interf. Sci. 114, 189–204.
Lagaly, G., Weiss, A., 1969. Van-der-waals interaction in dodecylammonium layer silicates. Z. Naturforsch. B 24, 1057-&.
Lagaly, G., Weiss, A., 1971. Arrangement and orientation of cationic tensides on silicate surfaces. 4. Arrangement of alkylammonium ions in low-charged silicates of films. Kolloid Z. Z. Polym. 243, 48-&.
Liu, X.D., Lu, X.C., Wang, R.C., Zhou, H.Q., Xu, S.J., 2007. Interlayer structure and dynamics of alkylammonium-intercalated smectites with and without water: a molecular dynamics study. Clays Clay Minerals 55, 554–564.
Liu, X., Lu, X.C., Wang, R.C., Zhou, H.Q., Xu, S.J., 2009. Molecular dynamics insight into the cointercalation of hexadecyltrimethyl-ammonium and acetate ions into smectites. Am. Mineral. 94, 143–150.
Liu, X.D., Meijer, E.J., Lu, X.C., Wang, R.C., 2010. Ab initio molecular dynamics study of Fe-containing smectites. Clays Clay Minerals 58, 89–96.
Liu, X.D., Lu, X.C., Wang, R.C., Zhou, H.Q., Xu, S.J., 2011. Speciation of gold in hydrosulphide-rich ore-forming fluids: insights from first-principles molecular dynamics simulations. Geochim. Cosmochim. Acta 75, 185–194.
Loewenstein, W., 1954. The distribution of aluminum in the tetrahedra of silicates and aluminates. Am. Mineral. 39, 92–96.
Meier, L.P., Nueesch, R., Madsen, F.T., 2001. Organic pillared clays. J. Colloid Interface Sci. 238, 24–32.
Ohtaki, H., Radnai, T., 1993. Structure and dynamics of hydrated ions. Chem. Rev. 93, 1157–1204.
Osman, M.A., Seyfang, G., Suter, U.W., 2000. Two-dimensional melting of alkane monolayers ionically bonded to mica. J. Phys. Chem. B 104, 4433–4439.
Osman, M.A., Ernst, M., Meier, B.H., Suter, U.W., 2002. Structure and molecular dynamics of alkane monolayers self-assembled on mica platelets. J. Phys. Chem. B 106, 653–662.
Osman, M.A., Ploetze, M., Skrabal, P., 2004. Structure and properties of alkylammonium monolayers self-assembled on montmorillonite platelets. J. Phys. Chem. B 108, 2580–2588.
Sheng, G.Y., Wang, X.R., Wu, S.N., Boyd, S.A., 1998. Enhanced sorption of organic contaminants by smectitic soils modified with a cationic surfactant. J. Environ. Qual. 27, 806–814.
Skipper, N.T., Refson, K., McConnell, J.D.C., 1991. Computer-simulation of interlayer water in 2-1 clays. J. Chem. Phys. 94, 7434–7445.
Smith, W., Forester, T., 1996. DL_POLY_2. 0: a general-purpose parallel molecular dynamics simulation package. J. Mol. Graph. 14, 136–141.
Smith, P., Lynden-Bell, R.M., Earnshaw, J.C., Smith, W., 1999. The surface-ordered phase of liquid heptadecane: a simulation study. Mol. Phys. 96, 249–257.
Stockmeyer, M., Kruse, K., 1991. Adsorption of zn and ni ions and phenol and diethylketones by bentonites of different organophilicities. Clay Miner. 26, 431–434.
Sun, H., 1995. Ab initio calculations and force field development for computer simulation of polysilanes. Macromolecules 28, 701–712.
Tambach, T.J., Hensen, E.J.M., Smit, B., 2004. Molecular simulations of swelling clay minerals. J. Phys. Chem. B 108, 7586–7596.
Tambach, T.J., Boek, E.S., Smit, B., 2006. Molecular order and disorder of surfactants in clay nanocomposites. Phys. Chem. Chem. Phys. 8, 2700–2702.
Tamura, K., Nakazawa, H., 1996. Intercalation of N-alkyltrimethylammonium into swelling fluoro-mica. Clays Clay Minerals 44, 501–505.
Vaia, R.A., Teukolsky, R.K., Giannelis, E.P., 1994. Interlayer structure and molecular environment of alkylammonium layered silicates. Chem. Mater. 6, 1017–1022.
Wang, L.Q., Liu, J., Exarhos, G.J., Flanigan, K.Y., Bordia, R., 2000. Conformation heterogeneity and mobility of surfactant molecules in intercalated clay minerals studied by solid-state NMR. J. Phys. Chem. B 104, 2810–2816.
Xu, S.H., Boyd, S.A., 1995a. Cationic surfactant adsorption by swelling and nonswelling layer silicates. Langmuir 11, 2508–2514.
Xu, S.H., Boyd, S.A., 1995b. Cationic surfactant sorption to a vermiculitic subsoil via hydrophobic bonding. Environ. Sci. Technol. 29, 312–320.
Yui, T., Yoshida, H., Tachibana, H., Tryk, D.A., Inoue, H., 2002. Intercalation of polyfluorinated surfactants into clay minerals and the characterization of the hybrid compounds. Langmuir 18, 891–896.
Zeitler, T.R., Greathouse, J.A., Cygan, R.T., 2012. Effects of thermodynamic ensembles and mineral surfaces on interfacial water structure. Phys. Chem. Chem. Phys. 14, 1728–1734.
Zeng, Q.H., Yu, A.B., 2008. Molecular dynamics simulations of organoclays and polymer nanocomposites. Int. J. Nanotechnol. 5, 277–290.
Zeng, Q.H., Yu, A.B., Lu, G.Q., Standish, R.K., 2003. Molecular dynamics simulation of organic-inorganic nanocomposites: layering behavior and interlayer structure of organoclays. Chem. Mater. 15, 4732–4738.
Zeng, Q.H., Yu, A.B., Lu, G.Q., Standish, R.K., 2004. Molecular dynamics simulation of the structural and dynamic properties of dioctadecyldimethyl ammoniums in organoclays. J. Phys. Chem. B 108, 10025–10033.
Zhou, Q., Lu, X.C., Liu, X.D., Zhang, L.H., He, H.P., Zhu, J.X., Yuan, P., 2011. Hydration of methane intercalated in Na-smectites with distinct layer charge: Insights from molecular simulations. J. Colloid Interface Sci. 355, 237–242.
Zhu, J.X., He, H.P., Zhu, L.Z., Wen, X.Y., Deng, F., 2005. Characterization of organic phases in the interlayer of montmorillonite using FTIR and C-13 NMR. J. Colloid Interface Sci. 286, 239–244.
Zhu, J.X., Zhu, L.Z., Zhu, R.L., Chen, B.L., 2008a. Microstructure of organo-bentonites in water and the effect of steric hindrance on the uptake of organic compounds. Clays Clay Minerals 56, 144–154.
Zhu, R., Zhu, L., Zhu, J., Xu, L., 2008b. Structure of surfactant-clay complexes and their sorptive characteristics toward HOCs. Sep. Purif. Technol. 63, 156–162.
Zhu, R., Molinari, M., Shapley, T.V., Parker, S.C., 2013. Modeling the interaction of nanoparticles with mineral surfaces: adsorbed C60 on pyrophyllite. J. Phys. Chem. A 117, 6602–6611.